Chapter 4

Plasma Formation Using a Double Saddle Coil Antenna

The use of the double saddle coil antenna has dominated helicon wave research since the early experiments by Boswell [14]. Until the present, very little was known about the coupling between the antenna and the plasma. All experimental systems, including the antenna configuration, were empirically designed. In order to design an antenna which will efficiently couple power to the plasma it is necessary to understand what modes will be excited by a particular antenna geometry - which will then determine the consequent plasma regime. Previous experimental measurements have been made of the wavefields, but only for a limited range of conditions and with ambiguous identification of wave modes.

This chapter describes detailed wavefield and plasma measurements over a wide parameter range, though only one frequency. A comparison is made between experimental measurements of dispersion and radiation resistance measurements and results from a

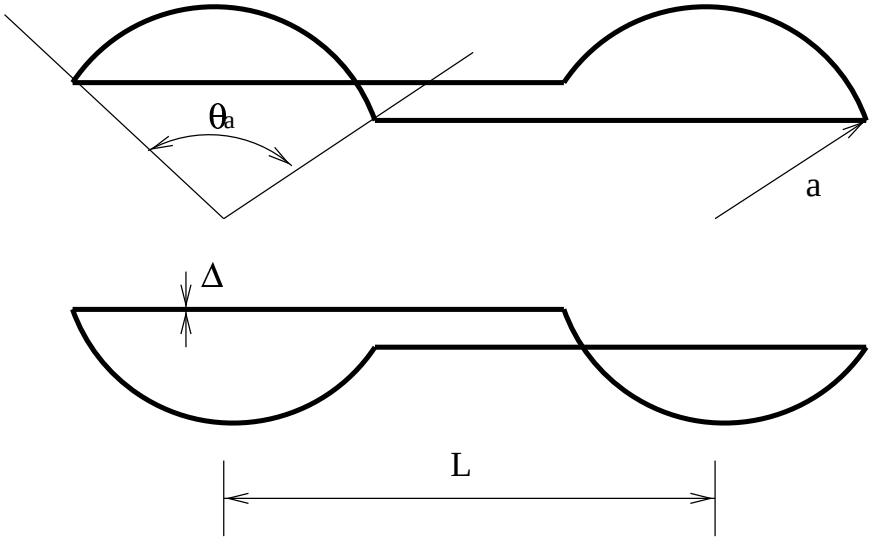

Figure 4.1: *Simplified double saddle coil antenna.*

MHD numerical model, and the implications for helicon wave discharges discussed.

4.1 Current Density of the Double Saddle Coil Antenna

To calculate the current density of the double saddle coil antenna the geometry is simplified by assuming the antenna consists of two current loops, with the currents flowing in phase as in figure 4.1.

The θ component of the current density can be written as

$$\begin{aligned} j_\theta(r,\theta,z) &= A\,[F\left(\frac{-\theta_a}{2} \le \theta \le \frac{+\theta_a}{2}\right) \\ &+ G\left(\frac{-\theta_a}{2}+\pi \le \theta \le \frac{+\theta_a}{2}+\pi\right) \\ &\times F\left(\frac{-L}{2}-\frac{\Delta}{2} \le z \le \frac{-L}{2}+\frac{\Delta}{2}\right) \\ &\times G\left(\frac{+L}{2}-\frac{\Delta}{2} \le z \le \frac{+L}{2}+\frac{\Delta}{2}\right)]\delta(r-a) \end{aligned} \tag{4.1}$$

where the functions F and G are defined as

$$F(X_1 \leq X \leq X_2) = \begin{cases} 1 & X \in [X_1, X_2] \\ 0 & X \ni [X_1, X_2] \end{cases} \tag{4.2}$$

$$G(X_1 \leq X \leq X_2) = \begin{cases} -1 & X \in [X_1, X_2] \\ 0 & X \ni [X_1, X_2] \end{cases} \tag{4.3}$$

and A is a constant that can be determined by integrating across the antenna. At $r = a$ and $\theta = 0^0$

$$I_{ant} = A \int_{\frac{L}{2}-\frac{\Delta}{2}}^{\frac{L}{2}+\frac{\Delta}{2}} dz \tag{4.4}$$

where I_{ant} is the antenna current, giving

$$A = \frac{I_{ant}}{\Delta} \tag{4.5}$$

Equation 4.1 can be Fourier transformed into the more useful coordinates of the azimuthal mode number m, and the wave number k.

$$\begin{aligned} j_\theta(r, m, k) &= \frac{4iI_{ant}}{k\Delta\pi m} \sin\left(\frac{k\Delta}{2}\right) \sin\left(\frac{m\theta_A}{2}\right) \\ &\times \sin\left(\frac{kL}{2}\right) (1 + \epsilon \cos m\pi) \delta(r - a) \end{aligned} \tag{4.6}$$

Examples of the wave number and the azimuthal wave number spectrums for a typical double saddle antenna can be seen in figure 4.2.

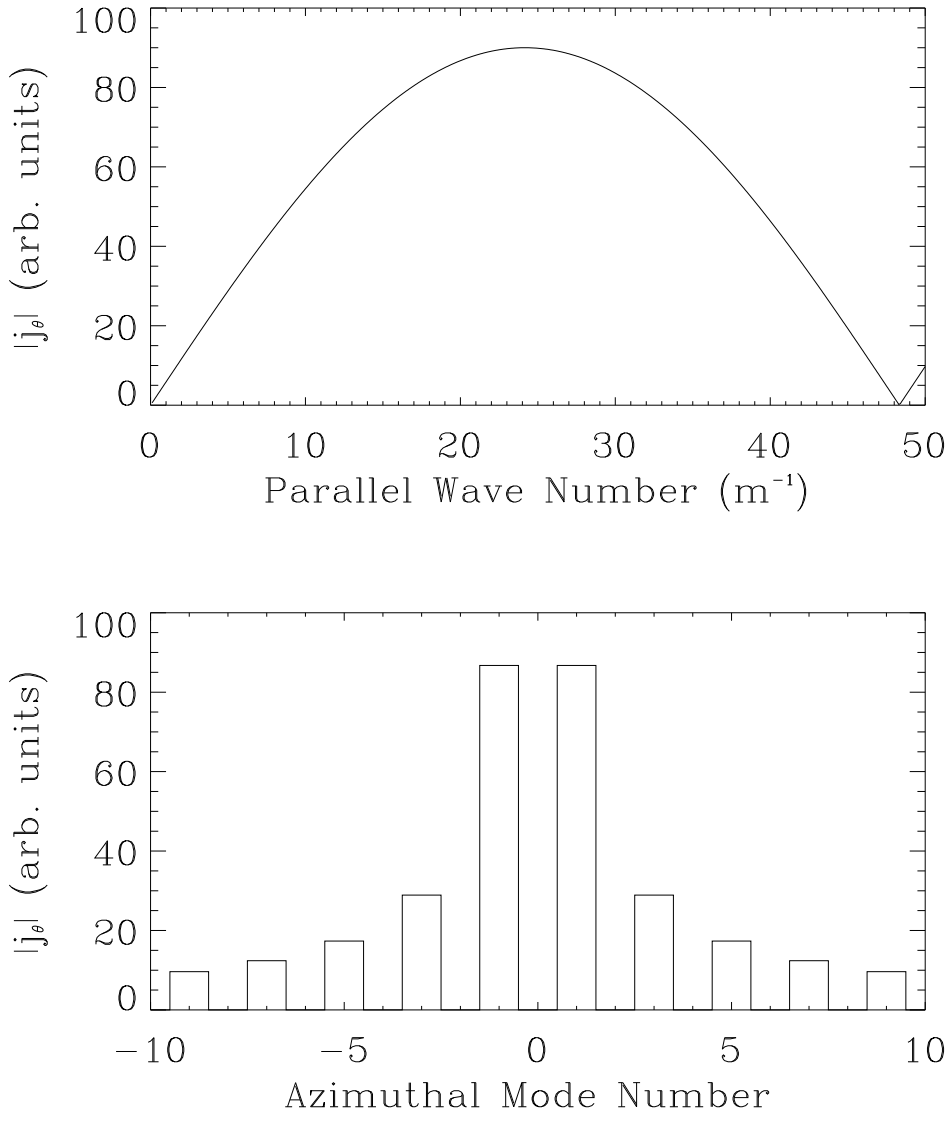

Figure 4.2: *The current density spectrum of the double saddle antenna,* $\Delta = 0.0034m$*,* $\theta_A = 90^0$*,* $r = 0.0225m$*, and* $L = 0.13m$*. (a) Axial spectra for azimuthal mode number* $m = +1$*. (b) Azimuthal mode number spectra for parallel wave number* $20m^{-1}$*.*

4.2 Discharge Time Evolution

Figure 4.3 shows the time evolution of the power into the matching box, antenna current, and radiation resistance. The discharge is characterised by two stages, the initial unstable stage and the equilibrium stage. During the early stage of the discharge the plasma diffuses away from the antenna along the field. This early stage is characterised by higher densities than in the late stage. An equilibrium is established once the density becomes reasonably uniform in the longitudinal direction and the overall density drops to a lower level. The physical processes of the initial stage of the discharge will be studied in chapter 6.

These two stages are characteristic of the discharge as can be seen in figures 4.4, 4.5, and 4.6, which show the time evolution of the power coupled to the plasma for various static fields using argon, neon, and helium respectively. Except for a few low power examples for argon, where it is not as obvious, an initial stage lasting many milliseconds, often over 10msec, can be seen. Comparisons with the numerical antenna coupling model are restricted to the late equilibrium stage of the discharge because the density is most uniform along the axis.

4.3 Longitudinal Wavefield Measurements

Measurements of the phase and amplitude of wavefields as a function of longitudinal position allow determination of wavelength and damping length. On axis measurements were made with a hooked probe inserted through an O-ring sealed end plate. The shaft of this probe lay along the inside of the Pyrex vacuum vessel and was terminated in a

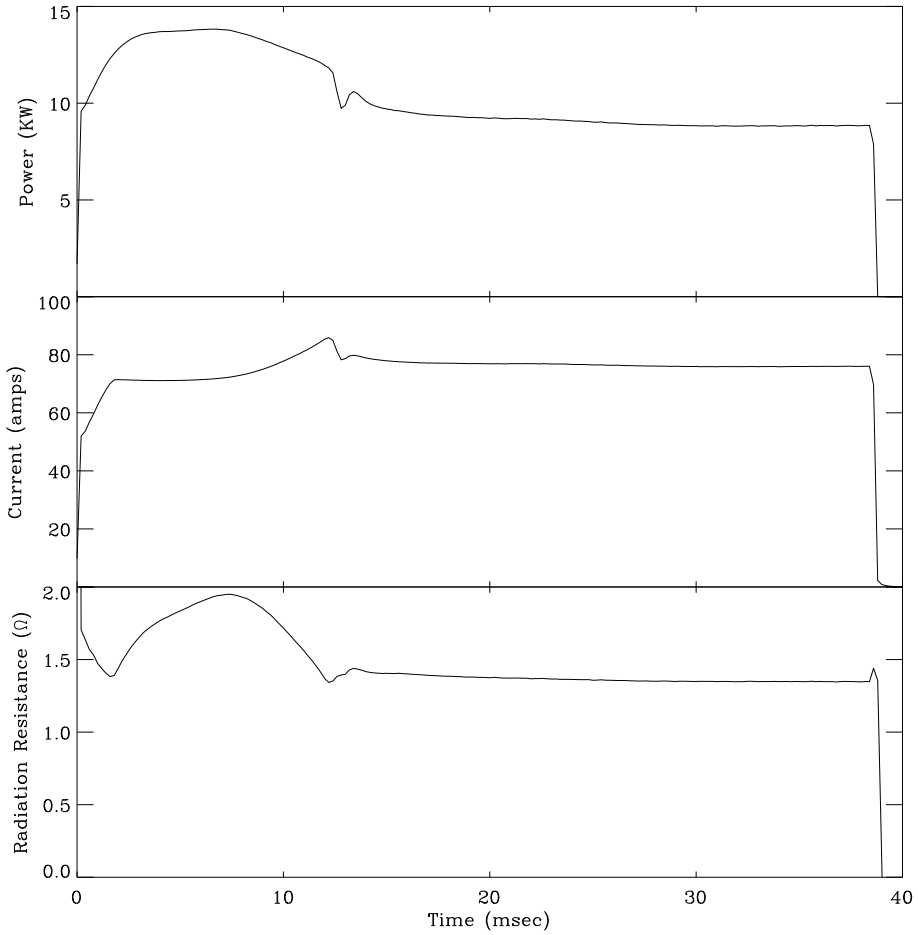

Figure 4.3: *(a) Power into the matching network (b) antenna current (c) radiation resistance for argon with a double saddle coil antenna at a static field of 896 gauss and filling pressure of 30mTorr.*

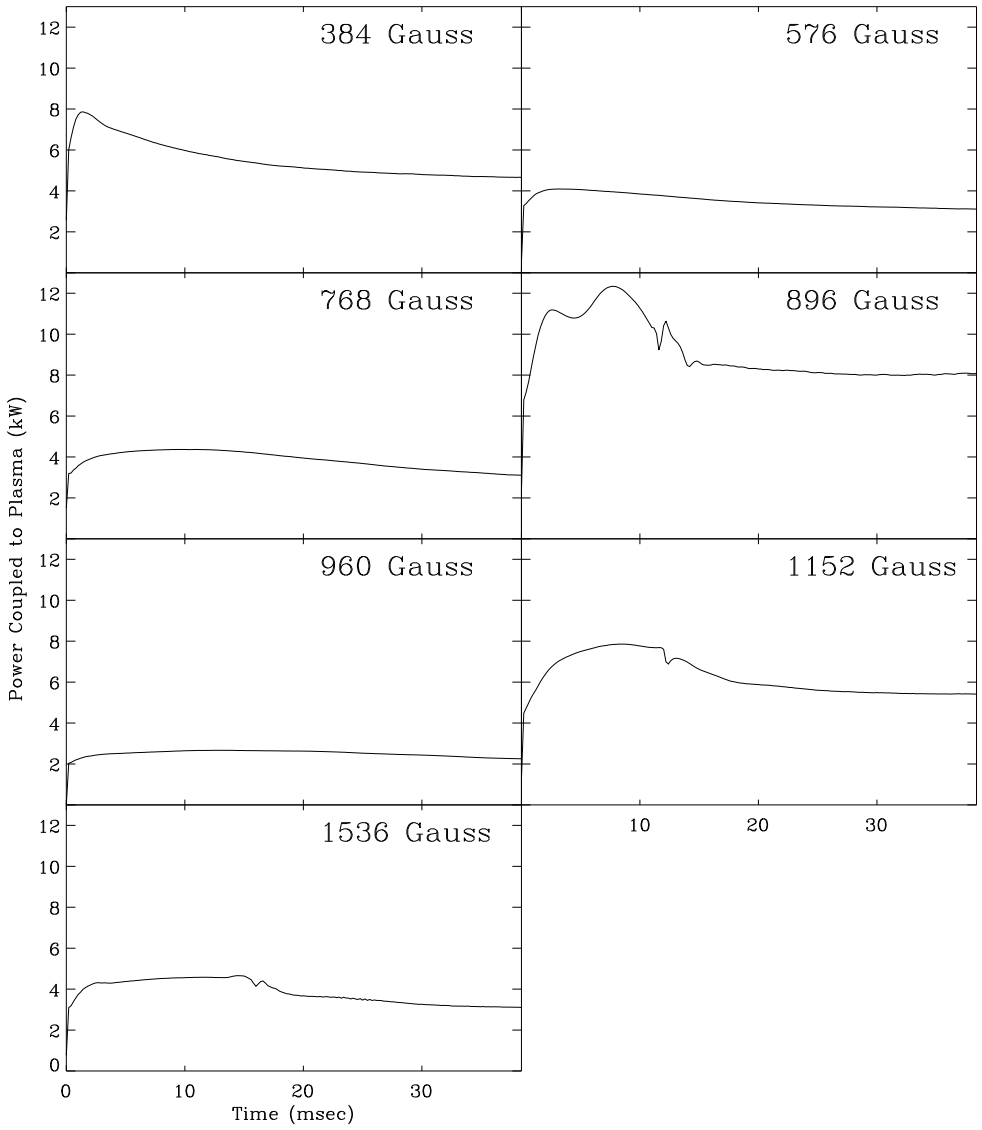

Figure 4.4: *Time evolution of the power coupled to the plasma at different static fields for argon.*

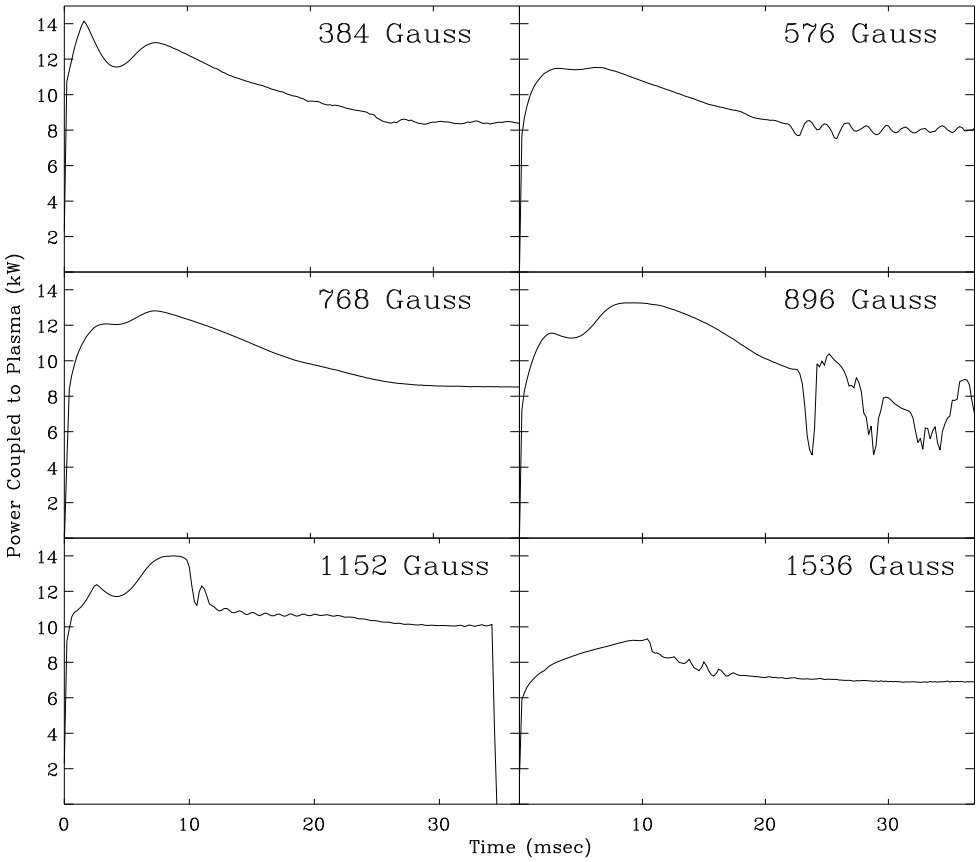

Figure 4.5: *Time evolution of the power coupled to the plasma at different static fields for neon.*

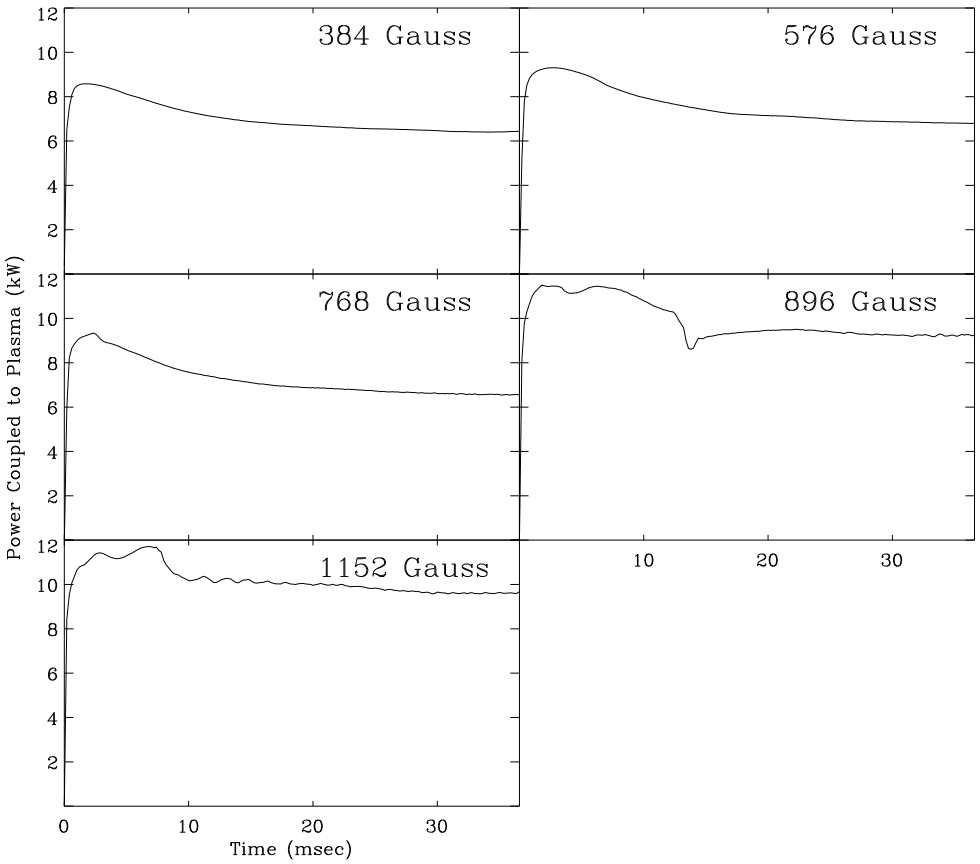

Figure 4.6: *Time evolution of the power coupled to the plasma at different static fields for helium.*

Langmuir probe and a 3 component magnetic probe 3cm apart. It was found that this probe significantly disturbed plasma produced by the double saddle coil antenna. When the probe was used, plasma perturbations were monitored using the floating potential of the radial probe placed on axis. Using a set of plasma conditions which were reasonably robust, and not overly disturbed by the probe, a complete set of on-axis measurements were made, with early and late stage measurements shown in figures 4.7 and 4.8.

Longitudinal wavefield measurements could also be made by drawing the azimuthal probe array along the vacuum vessel. The wavelength measurements taken by the azimuthal and axial probes agreed very well, as expected from simple wave theory. Thus all wavelengths were determined by the azimuthal array, which had the advantage of not disturbing the plasma. The wavelength was determined by Fourier analysis of the amplitude and phase of each of the array elements individually and averaging the results. In some cases more than one wavelength was evident in the early stage of the discharge. The advantage of this technique compared with measuring the slope of the phase is that, with the latter method, there are significant errors caused by interference by other wave numbers. The Fourier technique was also used to determine the parallel wave number in the numerical model.

Figures 4.7 and 4.8 present results from the early and late stage of the discharge. In the early stage the plasma has not reached an equilibrium and the plasma density is high. There is also a large density hump at the end of the discharge even though the apparent wave energy density is negligible in this region (this is discussed in chapter 6). Corresponding to the higher density measured in the initial stage of the discharge, the average wavelength is shorter than at the later time when equilibrium has been reached.

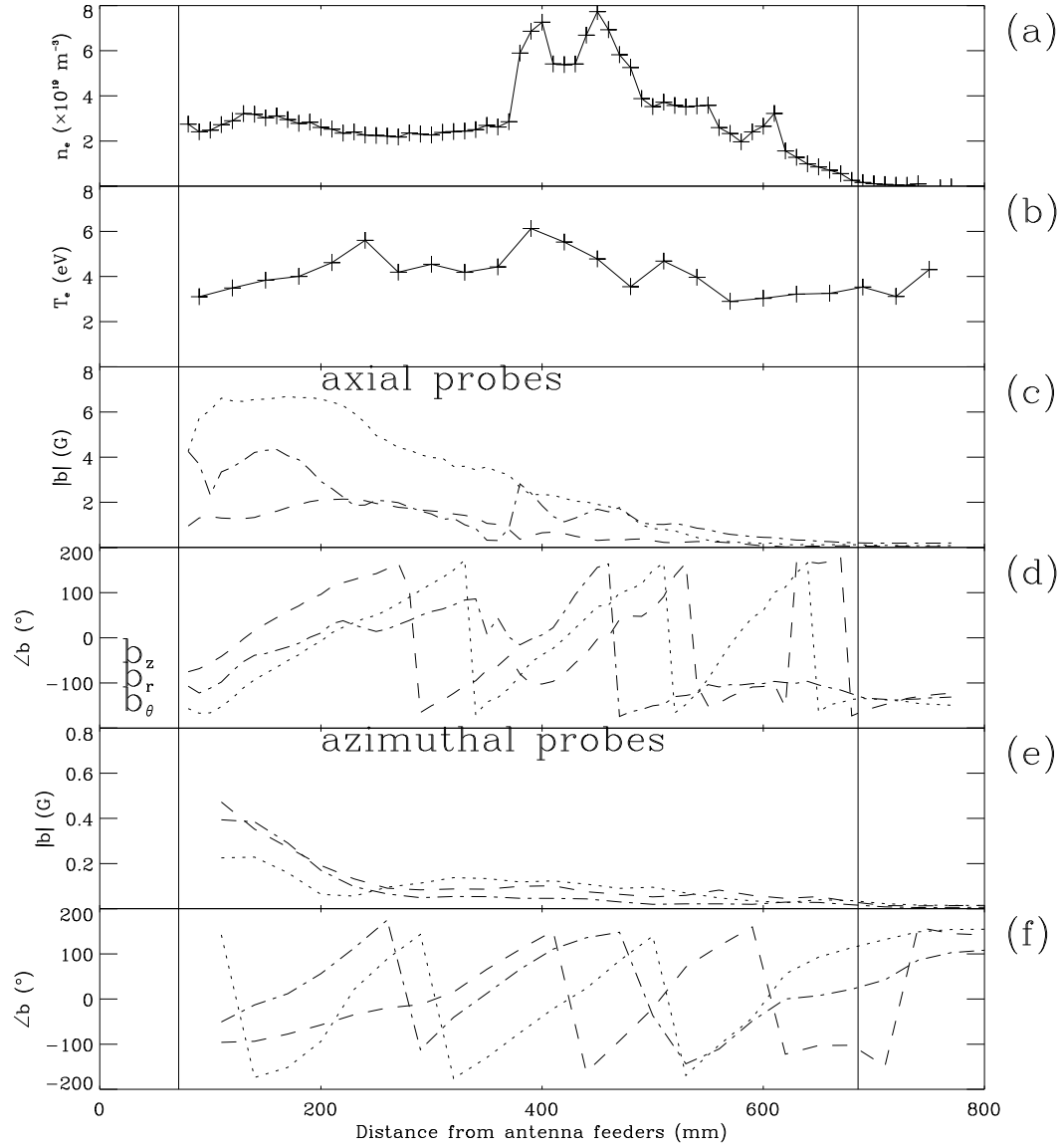

Figure 4.7: *Longitudinal measurements of (a) electron density (b) and temperature on axis (c) axial magnetic wavefield amplitudes and (c) phase and (d) 3 azimuthal magnetic wavefield amplitudes and (e) phase. Plots are shown 4msec into an argon discharge with a double saddle coil antenna at a static field of 1024 gauss and filling pressure of 7mTorr. The line at 150mm indicates the end of the antenna and the line at 700mm the end of the field coils.*

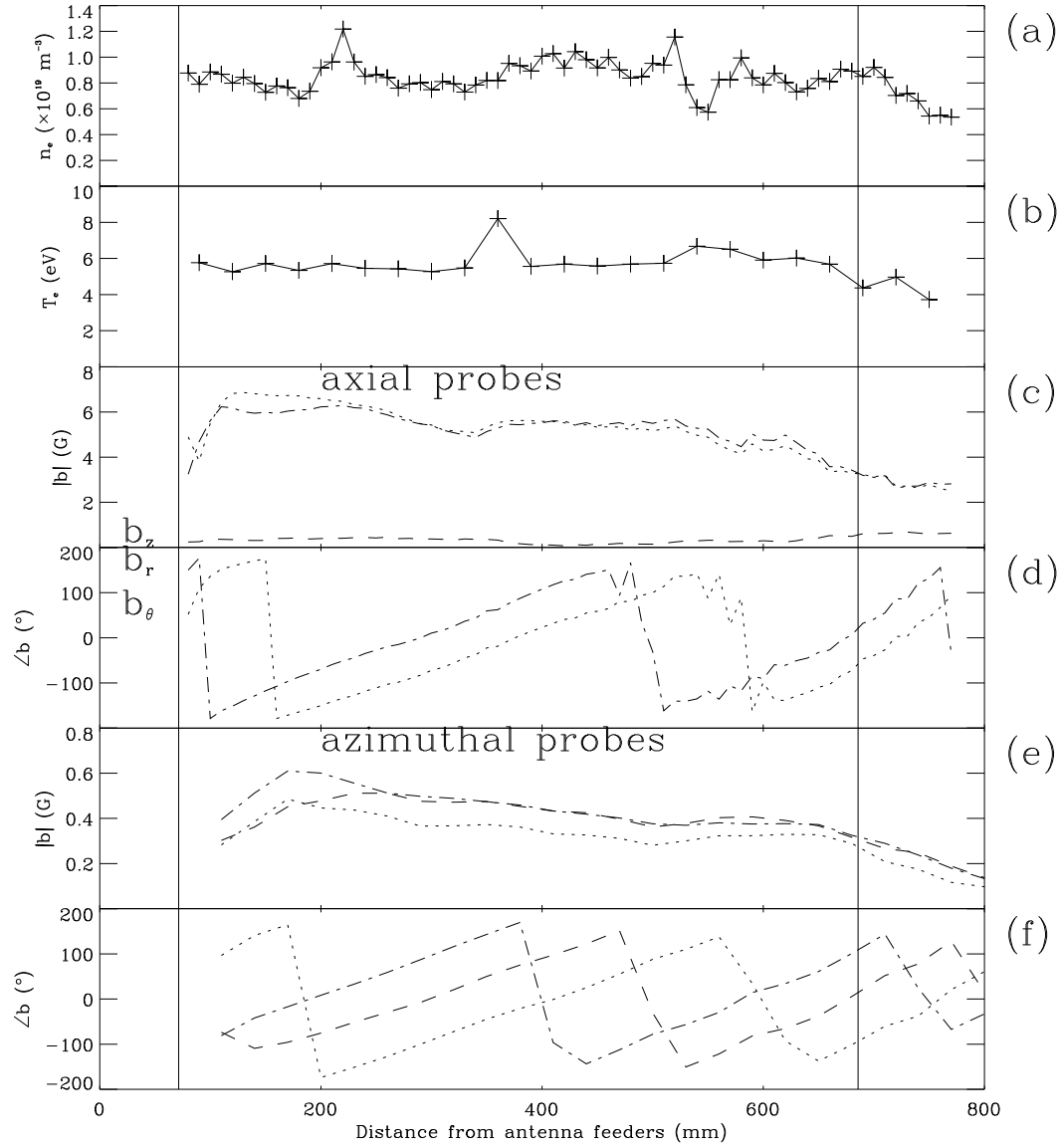

Figure 4.8: *Longitudinal measurements of (a) electron density (b) and temperature on axis (c) axial magnetic wavefield amplitudes and (c) phase and (d) 3 azimuthal magnetic wavefield amplitudes and (e) phase. Plots are shown 30msec into an argon discharge with a double saddle coil antenna at a static field of 1024 gauss and filling pressure of 7mTorr. The line at 150mm indicates the end of the antenna and the line at 700mm the end of the field coils*

The shortest wavelengths are measured in the region of the density peak. This agrees with similar axial measurements by Chen et al [32] in which the wavelength scales inversely with increasing axial density. In the latter case the density has dropped and the wavelength has correspondingly increased. The on axis wavefields have become dominated by the r and θ components, but the z component has become very small, which is consistent with an $m = +1$ azimuthal mode as confirmed by the azimuthal probe. The wavefields are more heavily damped in the early stage, consistent with higher collision frequencies at higher densities.

4.4 Azimuthal Magnetic Wavefields

The main deficiency in previous helicon measurements has been the lack of azimuthal profiles for the direct identification of azimuthal mode numbers. Azimuthal profiles for mode identification were also performed recently by Ellingboe and Boswell [48], who used a hooked magnetic probe inserted axially and rotated azimuthally. The double saddle coil antenna has no preference for azimuthal sign and while the $m = |1|$ modes dominate, the $m = |3|$ modes are not insignificant. One would then expect the azimuthal profiles to be a key diagnostic in determining which helicon mode occurs experimentally. Until now comparison with the dispersion relation (usually calculated for a uniform plasmas) and radial wavefield profiles have been used for mode identification. Due to the intrusive nature of magnetic probes, the technically difficult nature of making them small and avoiding (or, in our case, rejecting) capacitive coupling to the electric wavefield, their use has been limited to radial profiles and sparse longitudinal measurements for the de-

termination of $k_{||}$. These indirect means of determining azimuthal modes have a large uncertainty, making their use of limited value.

For Basil it was decided to attempt a direct measurement of azimuthal profiles with an array of 8 theta component probes on the outside of the Pyrex vacuum vessel. While this avoids using an intrusive probe it has the disadvantage of measuring the edge of the wavefields outside the plasma. Since the amplitude of the fields in Basil is of the order of a few gauss, the measurement techniques described in chapter 2 is reliable for most modes. However this technique has only limited capabilities to measure modes such as $m = 0$, the theta component of which is small at the plasma boundary. It is very reliable for resolving the $m = \pm 1$ modes. Thus azimuthal profiles are not reliable for determining the overall percentage make up of the total wave, but when moved axially, do allow unambiguous determination of wavelengths for different mode numbers.

The effects of the near field of the antenna on the azimuthal probe were determined by taking measurements with a typical antenna current but very low filling pressure. The antenna near field was found to be less than 5% of typical wavefields 10cm from the antenna. By Fourier analysing the data the azimuthal mode amplitudes were determined. The azimuthal array was also drawn along the tube for longitudinal measurements which were used to determine wavelengths and damping lengths for individual azimuthal modes.

All measurements in the stable late stage of the discharge show a very strong dominance of the $m = +1$ mode. Two examples are shown in figures 4.9 and 4.10. These examples are used as they span a wide parameter regime but still show identical features. Figure 4.11 is an azimuthal profile taken during the early stage of the discharge. While the simple antenna used in the numerical model has no $m = +2$ mode component this

mode dominates the experimentally measured spectra. This mode is probably produced by the complex azimuthal feeder arrangement, or the asymmetry in the sizes of the two loops of the double saddle coil antenna. The asymmetry in the sizes of the two loops of the double saddle coil antenna might look like a single side loop, which is capable of launching even mode numbers. The current density spectra of a single side loop has an $m = +2$ component almost as large as $m = 1$.

4.5 Radial Profiles of the Wavefields

Along with azimuthal modes there is the possibility of higher order radial modes. To help identify radial modes, radial profile measurements were made with a three component magnetic probe. Being an intrusive probe 5mm in diameter it caused some disturbance to the plasma. This was usually more pronounced once the probe had passed through the centre of the plasma. Despite this the probe produced some very good and useful results, a good example is given in figure 4.12 which shows characteristics of a pure $m = +1$ first radial mode discharge. B_z approaches 0 on axis, but stays finite due to the size of the probe and has a phase jump at the centre. In figure 4.12 the amplitudes of B_r and B_θ are very close to equal on axis as expected (this is also the case for the longitudinal axial measurements in figure 4.8). However, this is not the case in the radial profiles shown in figure 4.13, which is probably an indication of the perturbing effects of the probe.

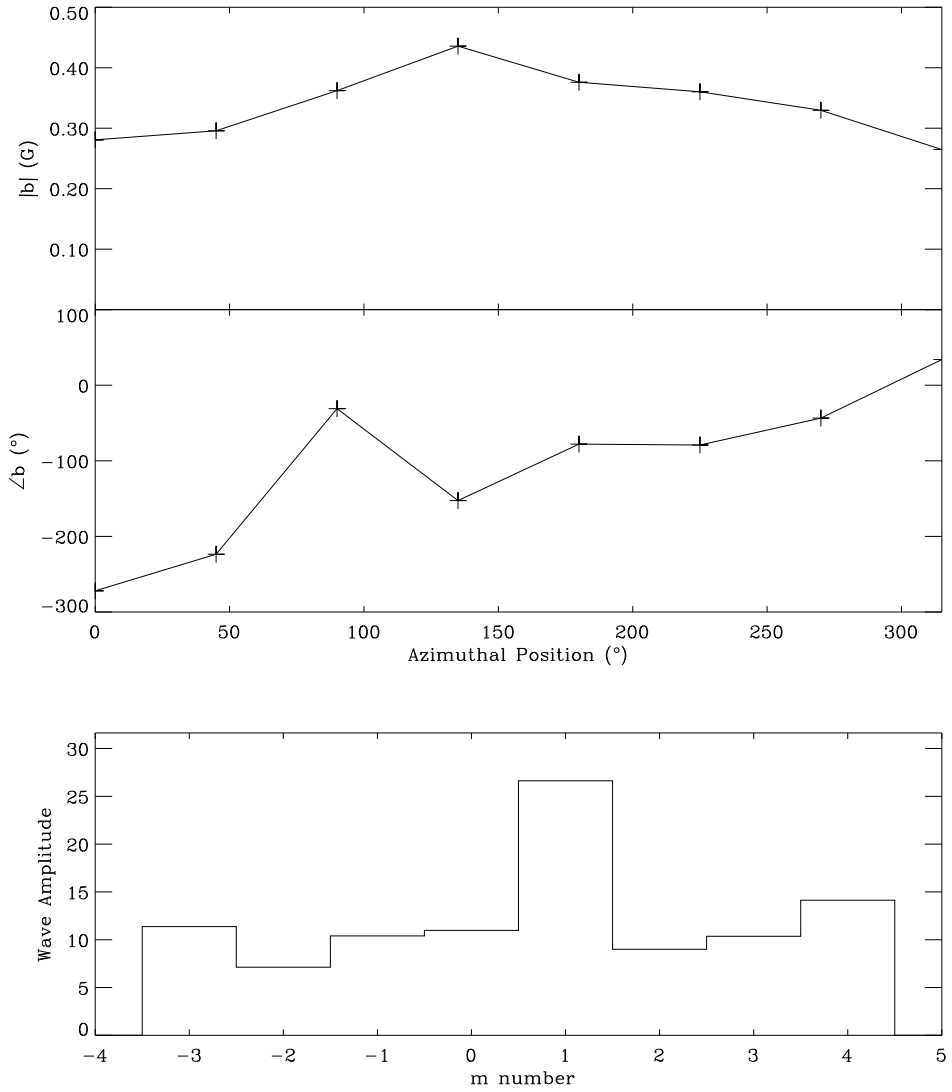

Figure 4.9: *Azimuthal measurements of (a) magnetic wave amplitude and (b) phase and the Fourier analysis of this data, 30msec into an argon discharge with a double saddle coil antenna at a static field of 1024 gauss and filling pressure of 7mTorr.*

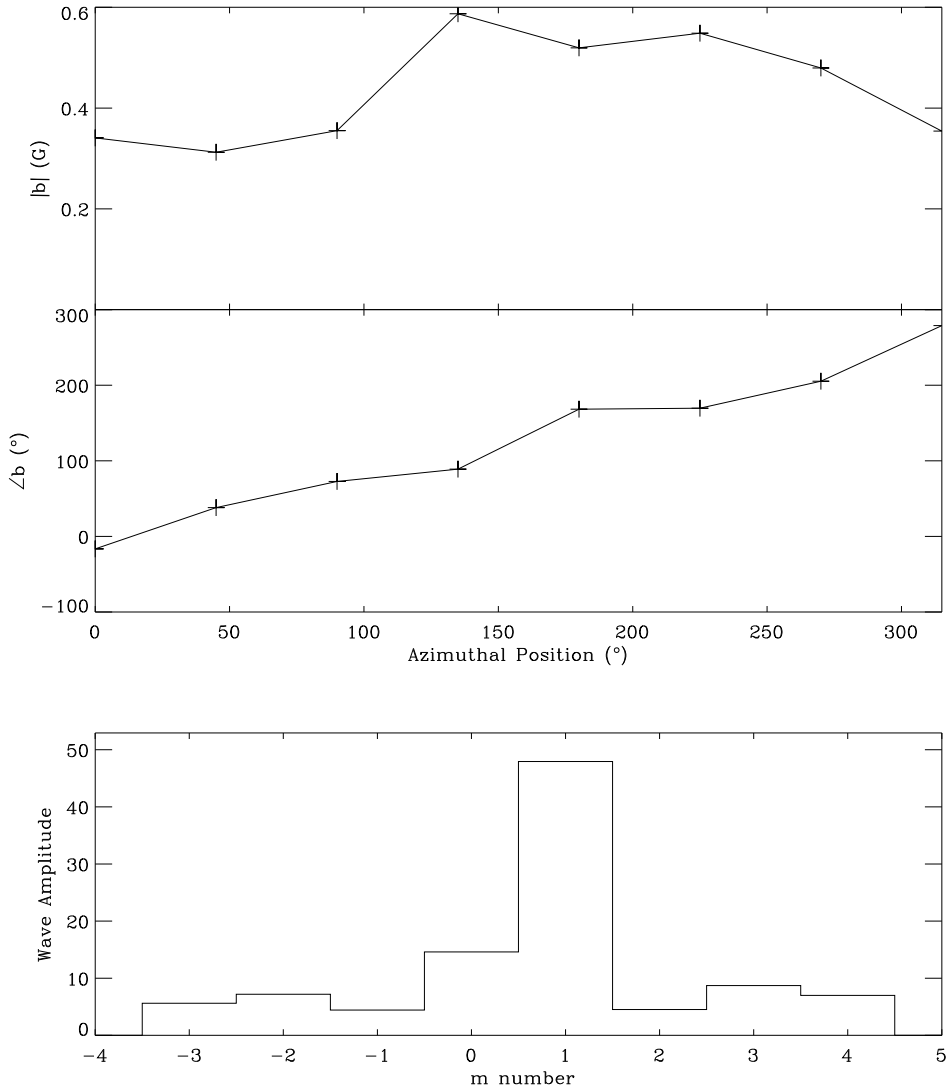

Figure 4.10: *Azimuthal measurements of (a) magnetic wave amplitude and (b) phase and the Fourier analysis of this data, 30msec into an argon discharge with a double saddle coil antenna at a static field of 896 gauss and filling pressure of 30mTorr.*

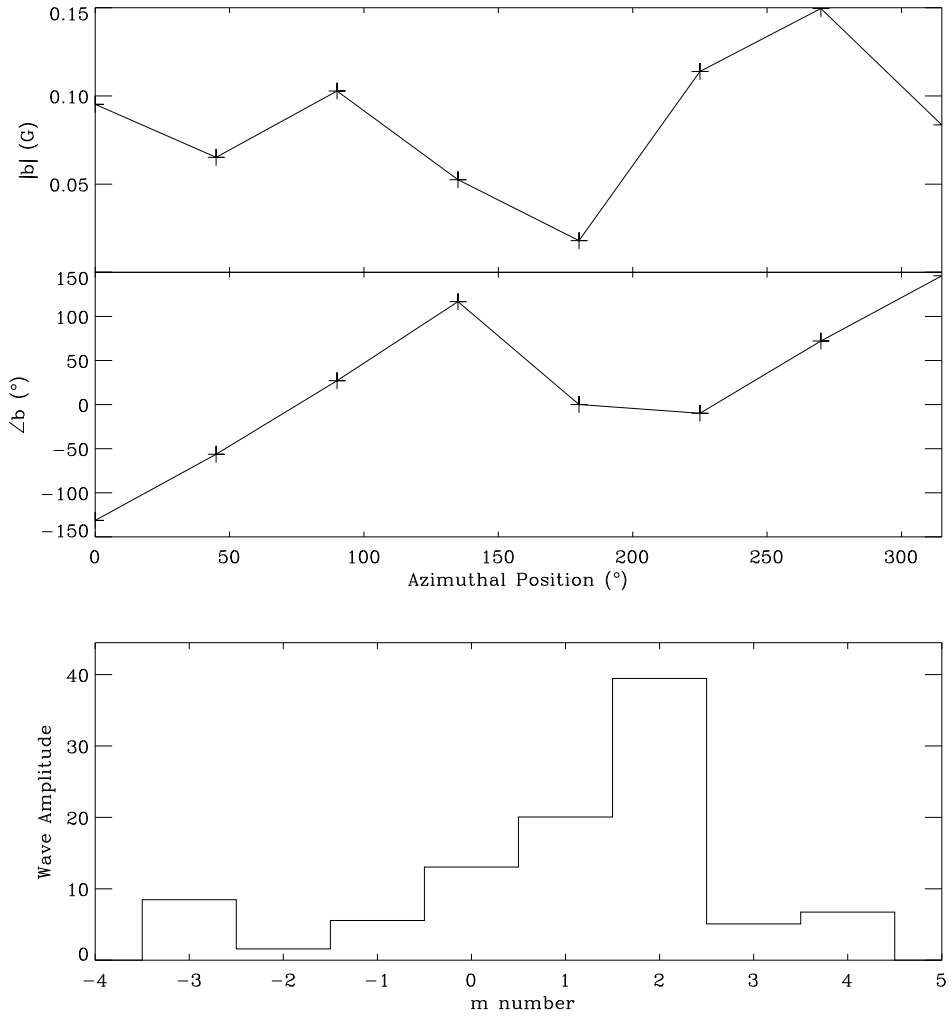

Figure 4.11: *Azimuthal measurements of (a) magnetic wave amplitude and (b) phase and the Fourier analysis of this data, 5msec into an argon discharge with a double saddle coil antenna at a static field of 896 gauss and filling pressure of 30mTorr.*

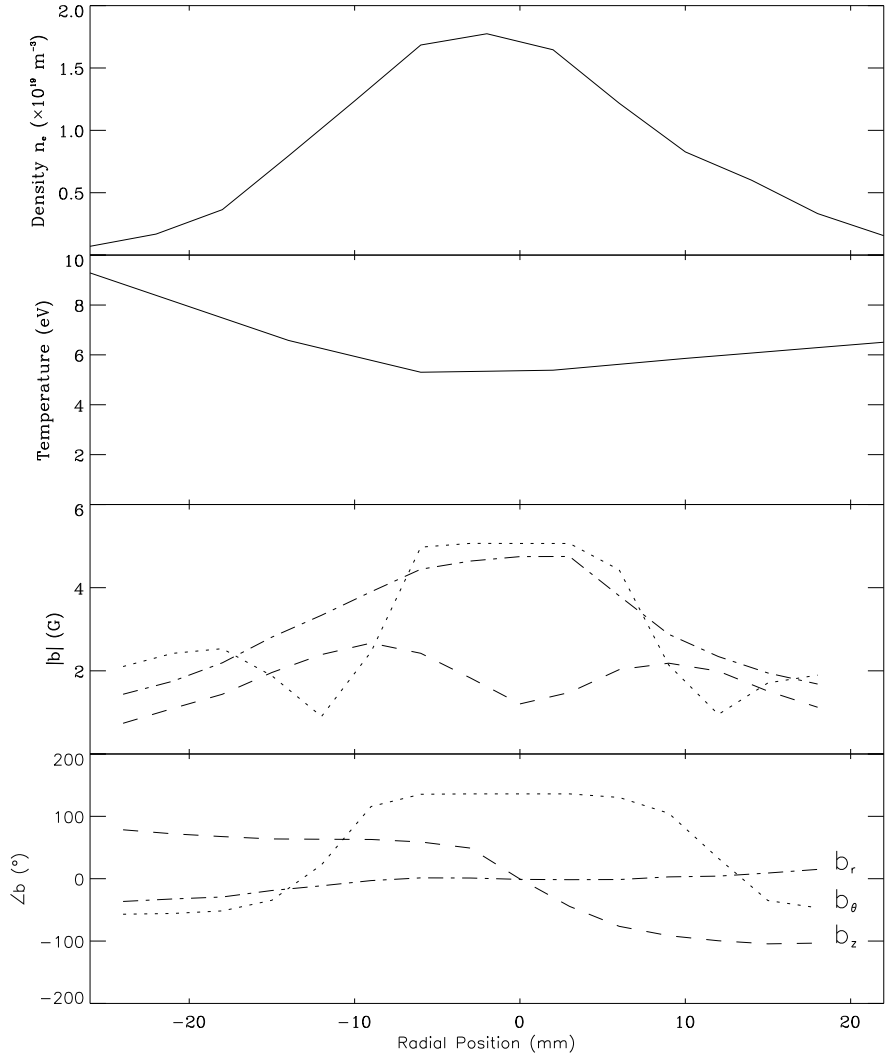

Figure 4.12: *Radial measurements of (a) electron density and (b) temperature and (c) magnetic wavefield amplitude and (d) phase, 30msec into an argon discharge with a double saddle coil antenna at a static field of 896 gauss and filling pressure of 30mTorr.*

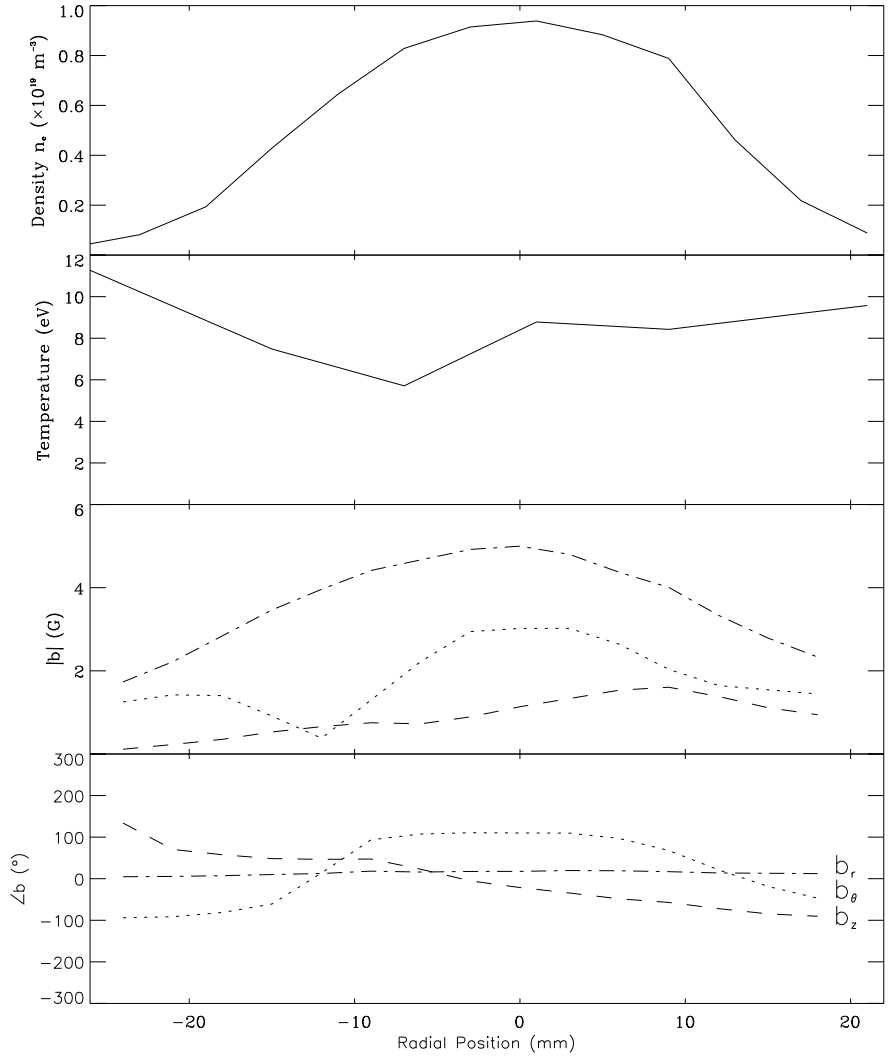

Figure 4.13: *Radial measurements of (a) electron density and (b) temperature and (c) magnetic wavefield amplitude and (d) phase, 30msec into an argon discharge with a double saddle coil antenna at a static field of 1024 gauss and filling pressure of 7mTorr.*

4.6 Wave Dispersion, Radiation Resistance, and Damping

In the latter stage of the discharge formed by the helicon wave, when the density becomes relatively uniform, it is possible to compare experimental measurements with the numerical model, which assumes longitudinal uniformity of the density. the model requires as input measurements of the plasma density profile in order to calculate wavelength and radiation resistance spectra. Examples of the measured profiles are shown for argon, neon, and helium at a range of magnetic fields in figures 4.14, 4.15, and 4.16. Although the radial profiles were only taken at one axial location, it is assumed that the profiles are similar along the tube.

Figure 4.17 compares the measured and calculated dispersion of the helicon wave. Note that this is not a dispersion "curve" as each modelled point is calculated for different density profiles. However it does closely resemble the simplified dispersion relation for a helicon wave propagating as an infinite plane wave with

$$k_{||} \approx \sqrt{\frac{n_e \omega \mu_0 e}{B_0}} \tag{4.7}$$

This is shown as the solid line in figure 4.17. A similar result was first obtained by Lehane and Thonemann [78]. However, these authors applied an unexplained multiplying factor to their density measurements. No correction factors have been included in the present results. The value for n_e used in equation 4.7 is the average density calculated by integrating under the density profile curve fitted to the experimental data, which was used

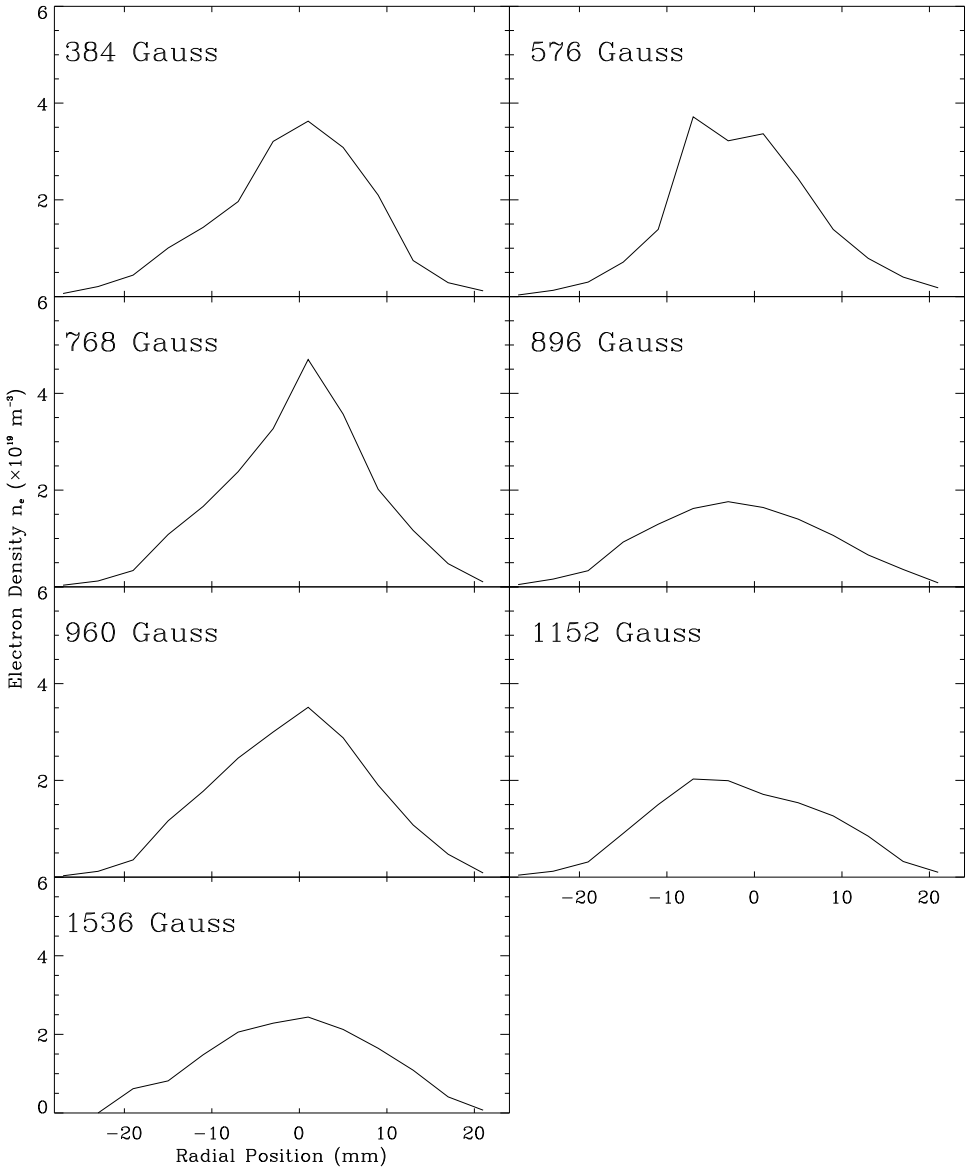

Figure 4.14: *Radial electron densities for argon with a double saddle coil antenna at different static fields late in the discharge.*

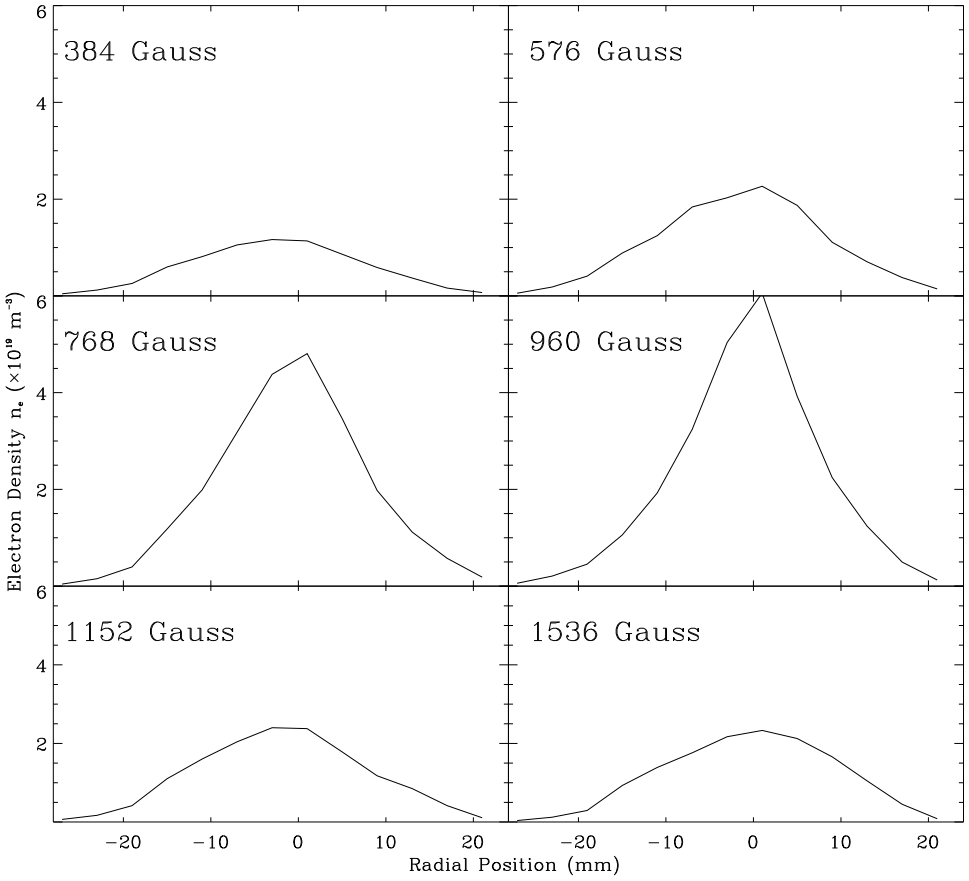

Figure 4.15: *Radial electron densities for neon with a double saddle coil antenna at different static fields late in the discharge.*

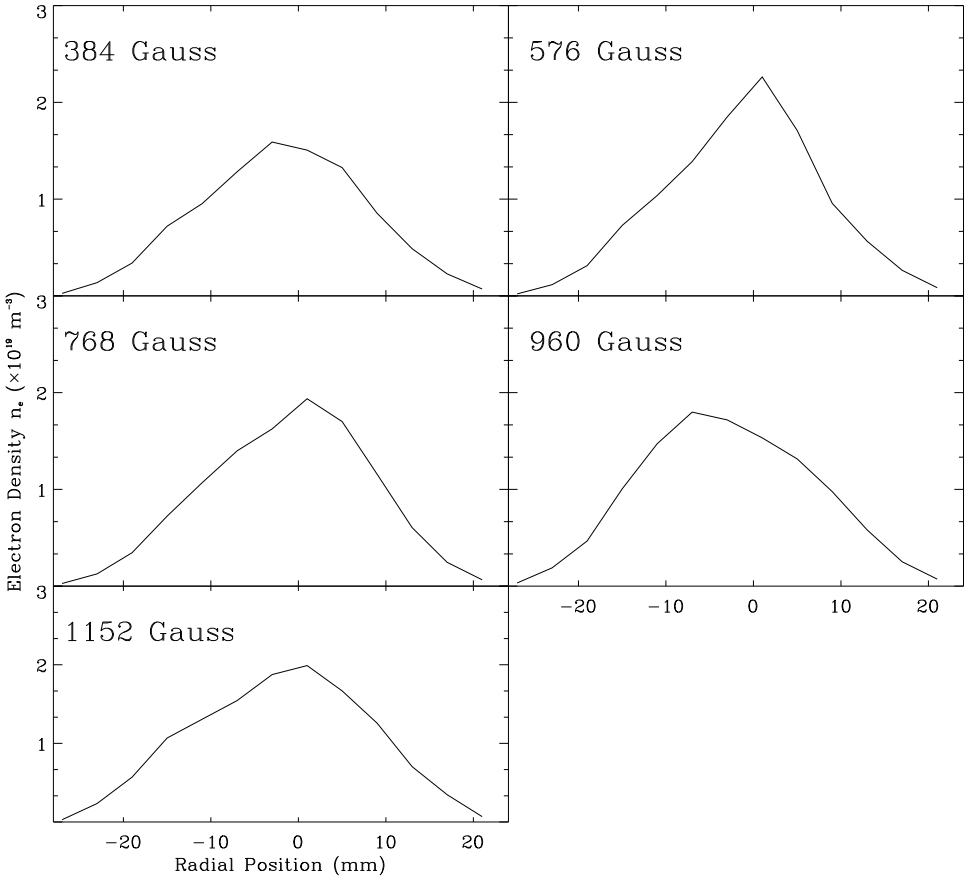

Figure 4.16: *Radial electron densities for helium with a double saddle coil antenna at different static fields late in the discharge.*

in the numerical model.

An interesting feature is that the wave appears to have no cutoff. This is explained by Kamenski and Borg [68] as being due to the $m = +1$ first radial mode propagating as a "surface" wave. The $m = 0$ and $m = +1$ second radial mode propagate as "body" waves, while the $m = +1$ first radial mode is a "surface" wave in a plasma with a vacuum boundary [39, 38]. This point is very important as detailed measurements have established the fact that the $m = +1$ mode has no cutoff, which is an important property for plasma formation. This has not been previously recognised, although previous authors [78, 42] have shown indirect evidence for the simple "infinite" plasma ($k_\perp \approx 0$) relation given in equation 4.7. All other work on helicon waves assumes or enforces a $k_\perp$ to determine $k_{||}$ from the relation

$$k_{||}\left(k_\perp^2 + k_{||}^2\right)^{\frac{1}{2}} = \frac{n_e \omega \mu_0 e}{B_0} \tag{4.8}$$

However for a small radius device like Basil, an estimate of an effective $k_\perp$, from the first non-zero root of the first order Bessel function, gives a large perpendicular wave number, $k_\perp \approx 150\text{m}^{-1}$, much larger than $k_{||}$. From equation 4.8 it might then be concluded that

$$k_{||}k_\perp \approx \frac{n_e \omega \mu_0 e}{B_0} \tag{4.9}$$

which does not agree with the results presented in figure 4.17.

In studying helicon waves most theory [70] has concentrated on understanding how different parameter limits effect wave dispersion and wavefield profiles. It is still poorly understood how the helicon wave maintains a plasma. Arguably the most important factor is how much energy can be coupled to the wave regardless of how it is dissipated in the

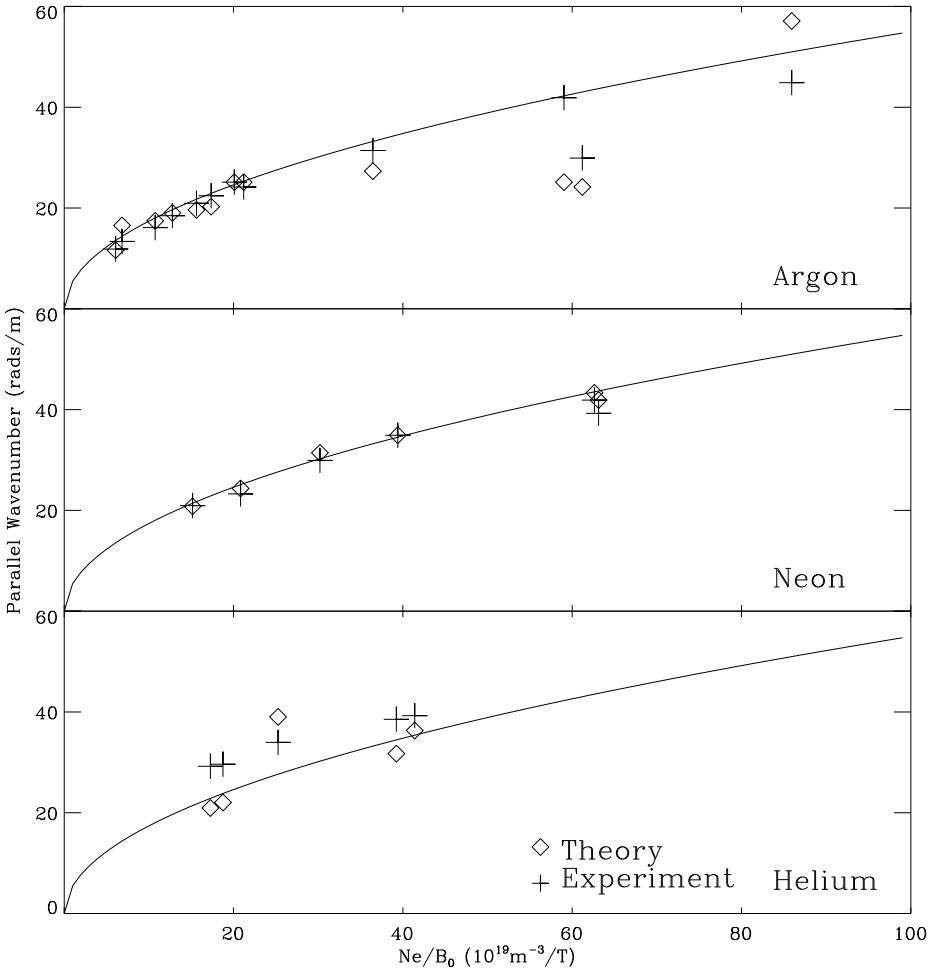

Figure 4.17: *Comparison of measured and calculated dispersion of the helicon wave launched by the double saddle coil antenna.*

plasma. Deciding what modes will be launched by an antenna has been limited to calculating the current density spectra of the antenna and concluding that any modes present in the antenna spectra are possibly coupled to the plasma. However, the modes launched by an antenna will depend on the ability of the antenna to couple power to these modes for the relevant plasma conditions. The power coupled to the wave from an antenna will be seen by the antenna as a resistance, i.e. the radiation resistance of the wave. The numerical MHD model by Kamenski [68] can calculate radiation resistance spectra of wave modes for a specified antenna and plasma conditions. Experimentally the total radiation resistance of all modes can be measured which can then be compared to the model results.

Figure 4.18 compares the measured and calculated radiation resistances for three gases. The agreement is quite satisfactory. It is concluded that the simple MHD numerical model produces reliable R_{ant} estimates. The good agreement suggests that the helicon wave is primarily responsible for the production of the plasma, since little power is left for the operation of parasitic mechanisms. According to the numerical model the $m = +1$ first radial mode dissipates over 90% of the radiated power for Basil conditions. This energy appears to be dissipated in the plasma by the propagating wave, and from the results shown in figure 4.8 the energy is deposited broadly along the machine. Moreover the power in the double saddle coil experiments ranged from 1kW to almost 10kW. Yet the linear theory of the numerical model still gave good agreement with the experimental radiation resistance measurements.

Over the range of filling pressure employed in Basil the plasma is highly collisional. This results in a highly damped wave. However, measurements of the damping are very difficult since highly damped waves do not propagate far past the near field of the antenna

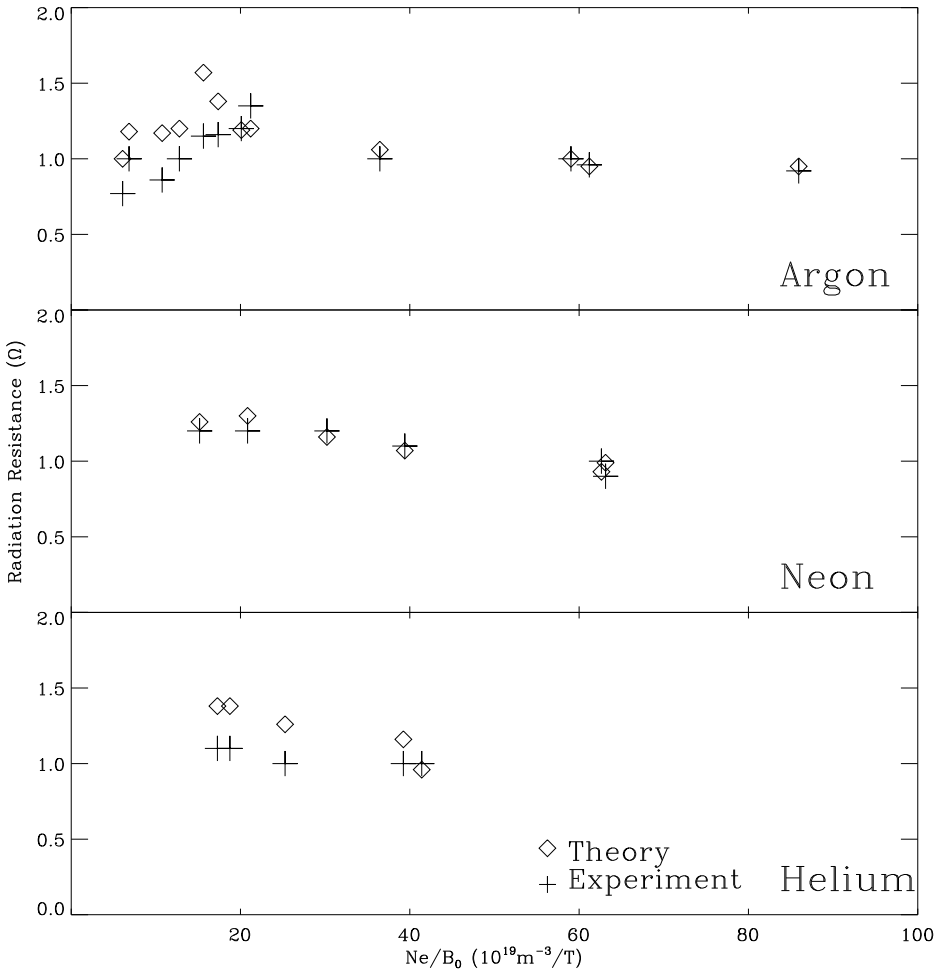

Figure 4.18: *Comparison between measured and calculated radiation resistance of the double saddle coil antenna.*

and so are difficult to identify and measurements of waves with low damping are complicated by the effects of the reflected wave at the end of the plasma. Figure 4.19 compares the measured damping with damping calculated due to a combination of electron-ion, electron-neutral collisions, and Landau damping. The calculation of collisional and Landau damping uses the results of section 3.4. Collisional damping is dominant with both collision frequencies being approximately equal, while the effective Landau collision frequency comprises less than 15% of the total. It is very noticeable that the damping is much stronger at high values of n_e/B_0, which is consistent with the collisional nature of the plasma and the increase of the collision frequency increasing with density.

In all results no adjustable parameters have been used to make the comparisons between experiment and theory. However, there is the possibility of considerable systematic errors in the experimental results. Estimation of errors in experimental results, such as Langmuir probe measurements, is very difficult and measurements of the density, which could not be calibrated against other diagnostics, could be expected to have systematic errors of up to 20%. This has important implications when these results are employed in the numerical model. It would be expected that results from the model for n_e/B_0 values which have a parallel wave number near the peak in the parallel wave number spectra should be less sensitive to errors than results where the current density spectra has the greatest slope. Thus the resultant error in the model results, due to any systematic errors in the experimental results, would be greatest for values away from $n_e/B_0 \approx 20 \times 10^{19}\mathrm{m}^{-3}\mathrm{T}^{-1}$ for the double saddle coil antenna used in the experiment. This is likely to explain why agreement between experimental and modelled values are good for low values of n_e/B_0, but decrease as $n_e/B_0 \rightarrow 100 \times 10^{19}\mathrm{m}^{-3}\mathrm{T}^{-1}$.

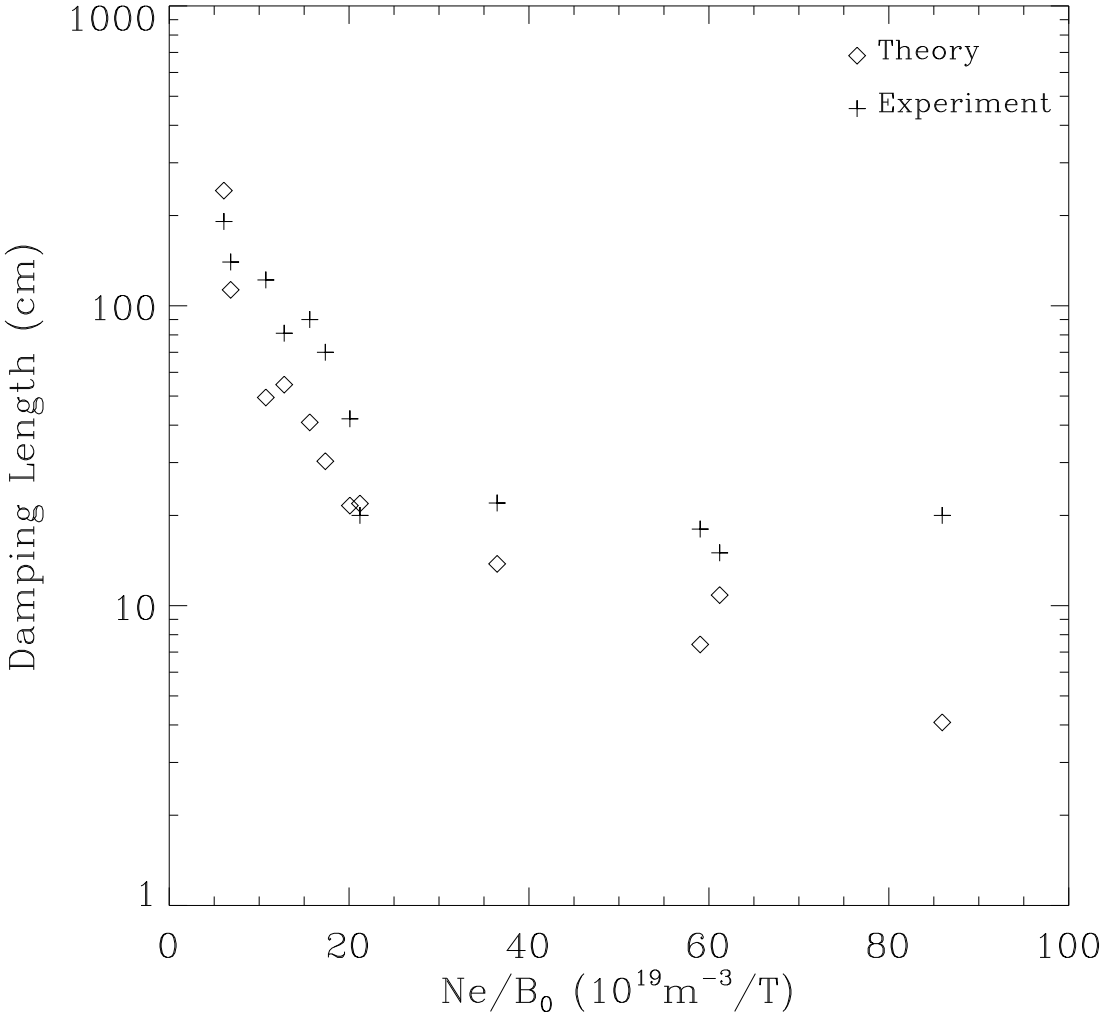

Figure 4.19: *Comparison between measured damping lengths and calculated damping lengths.*

4.7 Discussion

Kamenski [68] suggests that the inability of the double saddle coil antenna to launch the negative azimuthal modes, in particular the $m = -1$ mode, is due to two main factors: peaking of the density profile on axis, and the antenna being external to the plasma. Together these prevent the negative azimuthal modes from penetrating the plasma. In practice, $m = -1$ is more efficiently excited in large radius devices already used for plasma processing [48].

The radiation resistance is an important factor to consider in designing helicon plasma sources. The most obvious reason for maximising the radiation resistance is there will be a lower antenna current for a given power. This results in a reduction of the radiation resistive losses and lower antenna voltages in the matching network and antenna. The additional cost of cooling systems to a commercial processing machine can be considerable especially if water cooling is needed. In most helicon systems the antennas are very reactive and the usual limitation on the power applied to the antenna is due to insulation breakdown in matching network components. The average power is given by the current squared times the resistance, $P = I^2R$. Since the current is limited proportionally to the voltage, the only way to increase the power without increasing the voltage is by increasing the resistance. It must be emphasised that simply increasing the source power does not necessarily increase the power deposited into the plasma. Therefore reaching a desired density will depend on factors such as the ohmic losses in the matching network and the antenna length (since the radiation resistance decreases as the wavelength approaches the antenna length).

4.8 Summary

Detailed wavefield measurements of helicon waves launched by a double saddle coil antenna have been made in a long, high density plasma. In a discharge which has reached equilibrium a wave was found to propagate from the antenna and radial and azimuthal profiles were used to identify it as a single radial $m = +1$ azimuthal mode. No other significant modes were observed in the latter stages of the discharge, however in the early, high density stage $m = +2$ was observed. It is unclear why this mode is excited.

A numerical MHD model used measured radial plasma profiles to calculate the radiation resistance spectra of helicon waves launched by a double saddle coil antenna. The good agreement between measured and calculated radiation resistance confirms that the plasma is being produced by the deposition of power from the helicon wave. This conclusion is not in anyway altered by the damping rate of the wave. The dominance of the $m = +1$ mode can be explained by the high radiation resistance of this mode resulting in most of the power being coupled to it. Despite the non-equilibrium behaviour in the early phase of the discharge, the latter phase of the discharge wave physics appears to be well described by linear helicon wave theory.